Sum- and difference-frequency generation for broadband input fields

Y. B. Band,[1,2] C. Radzewicz,[2,*] and J. S. Krasinski[2]
[1]Department of Chemistry, Ben-Gurion University, Beer Sheva, Israel
[2]Department of Electrical Engineering and Computer Science, Oklahoma State University, Stillwater, Oklahoma 74078
(Received 31 March 1993)

We analyze the dynamics of sum-frequency generation (SFG) and difference-frequency generation (DFG) for broadband input fields. We demonstrate that amplitude modulation of the input fields significantly affects conversion efficiency of SFG and DFG, but frequency modulation does not affect conversion efficiency. Analytic results for SFG and DFG output-field intensities are thereby available for arbitrary fields. Self- and cross-phase modulation can affect the dynamics in the limit of very high field strengths, but these effects are of higher nonlinearity and therefore usually negligible. The quantum efficiency of DFG is shown to be generally higher than SFG, but the energy efficiency is much lower if the difference frequency is significantly less than the input frequencies. Optimal SFG quantum conversion efficiency for such systems approaches that of second-harmonic generation only if the quantum fluence (total number of photons) in the two input beams are equal. Optimal DFG quantum conversion efficiency occurs when the number of photons of frequency ω_2 is small yet sufficient for significant stimulation. A recently developed method for obtaining efficient SFG for multimode input fields is theoretically analyzed. The method involves using an arrangement with two or more nonlinear mixing crystals with a time-delay line situated between the crystals that delays one of the fundamental fields relative to the other. The efficiency in the second crystal depends on the cross-correlation function of the two fundamental fields upon leaving the first nonlinear crystal. The time-delay method is not effective for multimode DFG.

PACS number(s): 42.65.Ky

I. INTRODUCTION

In this paper we analyze and compare sum-frequency generation (SFG) and difference-frequency generation (DFG) for broadband input fields using the formulation of SFG and DFG for time-dependent input fields [1,2] (as opposed to cw single-frequency time-independent input fields). We analyze the efficiencies for these processes for arbitrary amplitude- and phase-modulated input fields and demonstrate that amplitude modulation of the fields significantly affects the conversion efficiency of SFG, DFG, and second-harmonic generation (SHG) but frequency modulation of the input fields does not affect the conversion efficiency. Nevertheless, self- and cross-phase modulation can affect the dynamics in the limit of very high field strengths, but these effects are of higher-order nonlinearity and therefore usually negligible. The description of SFG, DFG, and SHG for broadband input fields in Refs. [1,2] generalize the treatment of three-wave mixing for single-mode fields that was formulated in a classic paper by Armstrong *et al.* over 25 years ago [3] and is discussed in textbooks on nonlinear optics and quantum electronics [4–6]. In Refs. [1,2], analytic solutions were developed for the time-dependent intensities of the output fields for SFG and SHG when the input fields are amplitude modulated. These solutions differ dramatically from those for single-mode cw fields. New frequencies in the sum-frequency output spectra and the second-harmonic output spectrum, as well as in the output spectrum of the fundamental fields, are created and grow in magnitude as the input intensities are increased and/or the nonlinear susceptibility is increased. The applications of these ideas to intracavity SFG and SHG were also investigated [7]. Here we present the analytic description for DFG for amplitude-modulated input fields.

We have recently experimentally demonstrated [8] a scheme for improving the efficiency of SFG for broadband input fields based upon an approach first presented in Ref. [1]. The scheme involves using an arrangement with two or more nonlinear mixing crystals with a time-delay line for one of the fundamental fields, situated between the crystals. The delay line temporally shifts the fundamental fields one relative to another before they enter the next nonlinear crystal. The improvement in efficiency for SFG using the method is substantial while for DFG it is minimal, and might even be deleterious. Here, we analyze this method for improving SFG efficiencies and relate the efficiency with the cross-correlation function of the two fundamental fields after passing through the nonlinear crystal and before entering the next crystal, with and without the time-delay line.

Sum- and difference-frequency-generation conversion efficiencies are typically significantly less than the efficiency of SHG. For high SFG and DFG conversion

*Permanent address: Institute of Experimental Physics, University of Warsaw, Poland.

efficiency, the two input beams must be spatially and temporally matched. Spatial overlap is achieved by aligning the centers of the two input beams and using beams with the same beam diameter, divergence, and spatial mode structure. Temporal overlap is automatic for single longitudinal mode beams, and can be achieved for pulsed beams by overlapping the peaks of the pulses and assuring identical temporal profiles and pulse durations for both fields. For broadband fields with (central) frequencies ω_1 and ω_2, efficient SFG or DFG is difficult to achieve because mode-beating effects in each input field make it improbable that the instantaneous intensity of both fields is simultaneously high, and this is crucial for high conversion efficiency. Hence, when the intensity of both fields is low, the output power is low but the overall efficiency is not greatly affected, but when the intensity of one field is high and the other field is low, the photons in the intense field are wasted as far as frequency conversion is concerned. Highest SFG efficiencies are achieved when the number of photons in the two input fields are nearly equal. For SHG with a multimode laser source, when the instantaneous intensity of the fundamental frequency field is high, the intensity of the "other" field is also high by definition. In contrast to both SFG and SHG, DFG corresponds to the destruction of a photon at the high-frequency input field, say ω_1, and the simultaneous generation of a photon at idler frequency ω_2 as well as at the difference-frequency $\omega_3=\omega_1-\omega_2$. Hence the number of photons at the idler frequency need not be very plentiful, since they build up along with those at frequency ω_3, but their initial presence enhances the conversion process. The quantum efficiency of DFG is shown to generally be higher than SFG. The quantum efficiency of SFG approaches that of second-harmonic generation only if the quantum fluence (total number of photons) in the two input beams are equal, whereas the quantum efficiency of DFG is highest for the smallest number of photons of frequency ω_2, where the difference frequency equals $\omega_1-\omega_2$, provided a sufficient number of photons of frequency ω_2 are present to initiate DFG. The energy efficiency of DFG is, however, much less than SFG and SHG if the difference frequency is much less than the input frequencies.

The analysis here neglects group-velocity dispersion, self- and cross-phase modulation, and the spatial profile of the laser beams (i.e., a plane-wave assumption for the incident fields is made). Numerical calculations including these effects can be carried out to model particular experiments, but here we present the simplest picture in order to point out the essential physics of the SFG, DFG, and SHG processes and their differences.

In Sec. II we develop and compare the theoretical framework for treating SFG, DFG, and SHG for broadband input fields. Section III presents numerical studies of SFG and DFG for broadband input fields. Section IV contains the analysis of the method for obtaining improved efficiency of SFG for broadband input fields and correlates the improved efficiency to the cross-correlation function of the two fundamental fields upon leaving the first nonlinear crystal. In Sec. V we present a summary and conclusion.

II. THEORETICAL FRAMEWORK

We shall write the electric fields $F_i(x,t)$ in terms of a slowly varying envelope $E_i(x,t)$ and a phase given in terms of the central frequency ω_i and wave number k_i of field i,

$$F_i(x,t)=\exp[i(\omega_i t-k_i x)]E_i(x,t) .$$

The dynamical equations governing SFG of phase-matched plane waves are given in the slowly varying envelope approximation by

$$\begin{aligned}\frac{\partial E_1(z,\tau)}{\partial z}&=-i\frac{\omega_1}{n_1}\chi E_3 E_2^* ,\\ \frac{\partial E_2(z,\tau)}{\partial z}&=-i\frac{\omega_2}{n_2}\chi E_3 E_1^* ,\\ \frac{\partial E_3(z,\tau)}{\partial z}&=-i\frac{\omega_3}{n_3}\chi E_1 E_2 ,\end{aligned} \tag{1}$$

where E_1, E_2, and E_3 are the complex interacting electric field envelopes, ω_1, ω_2, and $\omega_3=\omega_1+\omega_2$ are their frequencies, n_i is the index of refraction of the medium at this frequency, $\tau=t-x/c$ is the local pulse time, $z=x$ is the distance in the medium, and χ is the nonlinear polarization coefficient for the three-wave mixing. The field envelopes satisfy the conservation equation:

$$\frac{\partial}{\partial z}\left[\frac{n_1|E_1|^2}{\omega_1}+\frac{n_2|E_2|^2}{\omega_2}+2\frac{n_3|E_3|^2}{\omega_3}\right]=0 . \tag{2}$$

This equation can be written in terms of the photon fluxes, $\Phi_i=cn_i|E_i|^2/\hbar\omega_i$ (in units of number of photons per unit area per unit second), in the form

$$\frac{\partial}{\partial z}(\Phi_1+\Phi_2+2\Phi_3)=0 . \tag{3}$$

The interpretation of this equation is that for every photon of frequency ω_3 that is created, two photons, one of frequency ω_1 and another at frequency ω_2, are destroyed. Equation (1) can be written in more symmetric form by defining the complex quantities $\phi_i=\sqrt{cn_i/\hbar\omega_i}E_i$, and takes the form

$$\begin{aligned}\frac{\partial\phi_1(z,\tau)}{\partial z}&=-i\chi'\phi_3\phi_2^* ,\\ \frac{\partial\phi_2(z,\tau)}{\partial z}&=-i\chi'\phi_3\phi_1^* ,\\ \frac{\partial\phi_3(z,\tau)}{\partial z}&=-i\chi'\phi_1\phi_2 ,\end{aligned} \tag{4}$$

where χ' is related to the SFG susceptibility χ by the equation $\chi'=\sqrt{\hbar^3\omega_1\omega_2\omega_3/c^3 n_1 n_2 n_3}\chi$. The magnitude of ϕ_i is the square root of the photon flux for field i, and its phase is the phase of the electric field.

The analytic solution for the intensity or the photon flux of these fields, for real χ and real slowly varying envelopes (i.e., amplitude-modulated fields), and the initial condition $\Phi_3(0,\tau)=0$, is

$$\Phi_3(z,\tau)=\Phi_{\min}(0,\tau)\mathrm{sn}^2\left[\sqrt{\Phi_{\max}(0,\tau)}\chi' z,\left[\frac{\Phi_{\min}(0,\tau)}{\Phi_{\max}(0,\tau)}\right]^{1/2}\right],$$
$$\Phi_1(z,\tau)=\Phi_1(0,\tau)-\Phi_3(z,\tau)\ ,\ \text{and}\ \ \Phi_2(z,\tau)=\Phi_2(0,\tau)-\Phi_3(z,\tau)\ . \tag{5}$$

Here sn(,) is the doubly periodic Jacobi elliptic function [9], $\Phi_{\min}(0,\tau)$ and $\Phi_{\max}(0,\tau)$ are the smaller and the larger input fields, $\Phi_1(0,\tau)$ and $\Phi_2(0,\tau)$, incident upon the sample at time τ. These solutions are appropriate even when fields 1 and 2 are multifrequency beams. The solution, Eq. (5), is valid provided the spectrum of the fields 1 and 2 remain within the phase-matching bandwidth throughout propagation in the crystal, and the input fields are not phase modulated. An analytic solution is not known for phase-modulated input fields. However, we show below that SFG and DFG for input fields with the same amplitude modulation, but with no phase modulation, have the same output intensities as the amplitude- and phase-modulated fields. That is, the output intensities of the fields are independent of the phase modulation of the input fields.

The dynamical equations governing DFG of phase-matched plane waves are given in the slowly-varying-envelope approximation by

$$\frac{\partial E_1(z,\tau)}{\partial z}=-i\frac{\omega_1}{n_1}\chi E_3 E_2\ ,$$
$$\frac{\partial E_2(z,\tau)}{\partial z}=-i\frac{\omega_2}{n_2}\chi E_3^* E_1\ , \tag{6}$$
$$\frac{\partial E_3(z,\tau)}{\partial z}=-i\frac{\omega_3}{n_3}\chi E_1 E_2^*\ ,$$

where E_1, E_2, and E_3 are the complex interacting electric fields, $\omega_1,\omega_2,\omega_3=\omega_1-\omega_2$. The conservation equation satisfied by the field envelopes is

$$\frac{\partial}{\partial z}\left[2\frac{n_1|E_1|^2}{\omega_1}+\frac{n_2|E_2|^2}{\omega_2}+\frac{n_3|E_3|^2}{\omega_3}\right]=0\ . \tag{7}$$

Written in terms of the photon fluxes, this equation takes the form

$$\frac{\partial}{\partial z}(2\Phi_1+\Phi_2+\Phi_3)=0\ . \tag{8}$$

The interpretation of this equation is that for every photon of frequency ω_1 that is destroyed, two photons, one at frequency ω_2 and another at frequency ω_3, are created. In terms of ϕ_i, Eq. (6) can be written as

$$\frac{\partial\phi_1(z,\tau)}{\partial z}=-i\chi'\phi_3\phi_2\ ,$$
$$\frac{\partial\phi_2(z,\tau)}{\partial z}=-i\chi'\phi_3^*\phi_1\ , \tag{9}$$
$$\frac{\partial\phi_3(z,\tau)}{\partial z}=-i\chi'\phi_1\phi_2^*\ .$$

The analytic solutions for the intensity or the photon flux of these fields for real χ and real slowly varying envelopes when the initial condition $\Phi_3(0,\tau)=0$ is imposed are

$$\Phi_1(z,\tau)=\Phi_1(0,\tau)\mathrm{cn}^2\left[\sqrt{\Phi_{\max}(0,\tau)}\chi' z,\left[\frac{\Phi_{\min}(0,\tau)}{\Phi_{\max}(0,\tau)}\right]^{1/2}\right],$$
$$\Phi_2(z,\tau)=\Phi_2(0,\tau)+[\Phi_1(0,\tau)-\Phi_1(z,\tau)]\ ,\ \text{and}\ \ \Phi_3(z,\tau)=\Phi_1(0,\tau)-\Phi_1(z,\tau)\ . \tag{10}$$

Let us begin our study of the dynamics of SFG and DFG by reviewing the nature of the propagation through the nonlinear crystal. We integrate the first-order differential equations (1) and (6) [or (4) and (9)] from $z=0$ given initial conditions $E_i(0,\tau)$ [or $\phi_i(0,\tau)$], with τ held constant. We first present the results for SFG. Figure 1 shows the photon fluxes at frequencies ω_1, ω_2, $\omega_3=\omega_1+\omega_2$, Φ_1, Φ_2, and Φ_3 versus propagation distance in the nonlinear crystal for two different initial ratios of $\Phi_1(z=0)$ and $\Phi_2(z=0)$, with the fields taken to be real, $\Phi_3(z=0)=0$, and $\chi'=1.0$. In Fig. 1(a) the initial photon flux at frequency ω_2 is one-tenth of the flux at frequency ω_1, $\Phi_2(0)=\Phi_1(0)/10$. The largest number of photons at frequency $\omega_1+\omega_2$ that can be created (obtained at $z\sim 0.35$) equals the number of photons at frequency ω_2 (the number of photons in the smallest input field). At $x\sim 0.35$, all the photons at frequency ω_2 have been used up and subsequently reconversion of $\omega_1+\omega_2$ photons to photons of frequency ω_1 and ω_2 begins to take place. The reconversion continues until all the photons at frequency $\omega_1+\omega_2$ are depleted. For $x>0.65$, the process of conversion and then reconversion cycles, i.e., the results are periodic with distance since sn(,) is periodic in its first argument. In Fig. 1(b) the initial photon flux at frequencies ω_1 and ω_2 are taken equal, $\Phi_1(0)=\Phi_2(0)$. This case is similar (but not identical [6]) to the case of SHG, where the number of photons of frequency ω_1 equals the number of photons of frequency $\omega_2(=\omega_1)$. In this case, no reconversion of photons of frequency $\omega_1+\omega_2$ to photons of frequency ω_1 and ω_2 is possible because, in order for the

reconversion to take place, photons at one of the initial frequencies must be present. Here, they have all been converted. The solution then degenerates into the familiar tanh solution, i.e., sn(,1)=tanh( ). We should point out, however, that the description of SFG is not equivalent to that of SHG even if the number of photons at frequencies ω_1 and ω_2 are equal [2]. This is due to the fact that the SFG formalism describes exclusively the interaction of photons from two different beams, and interaction of photons from the same bean is not present. In the degenerate SFG case, where $\omega_1=\omega_2$, any pair of photons, independent of their origin, can interact to generate the second harmonic.

Figure 2 is similar to Fig. 1, except here we consider DFG. From Fig. 2(a), which shows the case with initial flux ratio given by $\Phi_2(0)=\Phi_1(0)/10$, it is clear that as ω_1 photons are destroyed, ω_2 photons and $\omega_1-\omega_2$ photons are simultaneously created. Once ω_1 photons are depleted ($x\sim0.5$), reconversion of ω_2 and $\omega_1-\omega_2$ photons begins. At propagation distances larger than 1.0, the behavior is periodic and reproduces the results in the region [0,1]. In Fig. 2(b), the case with initial fluxes $\Phi_1(0)=\Phi_2(0)$ is shown. At $x\sim0.25$, all the ω_1 photons are used up and the photons at frequencies $\omega_1-\omega_2$ and ω_2 reconvert to form photons at frequency ω_1. Beyond $x=0.5$, the dynamics are periodic and reproduce the results shown in the region [0,0.5].

III. NUMERICAL STUDIES OF SFG AND DFG FOR BROADBAND INPUT FIELDS

We now consider time-dependent input fields. Propagation of multimode fields having both amplitude and phase modulation must be numerically treated. In what follows we consider the case where each input field (1 and 2) originates from a laser emitting at frequencies close to several cavity mode frequencies. The temporal dependence of the input electric fields can then be written as

$$F_i(0,\tau)=\sum_{j=-n}^{n} E_{i,j}\exp[i(\omega_{i,j}\tau+\theta_{i,j})]$$

$$=\exp[i\omega_i\tau]\sum_{j=-n}^{n} E_{i,j}\exp[i(j\Delta_i\tau+\theta_{i,j})]$$

$$\text{for } i=1,2\ , \quad (11)$$

where $\omega_{i,j}=\omega_i+j\Delta_i$, ω_i is the central frequency of the ith field, Δ_i is the mode frequency spacing of cavity i ($=c/L_i$, where L_i is the round-trip optical length of the

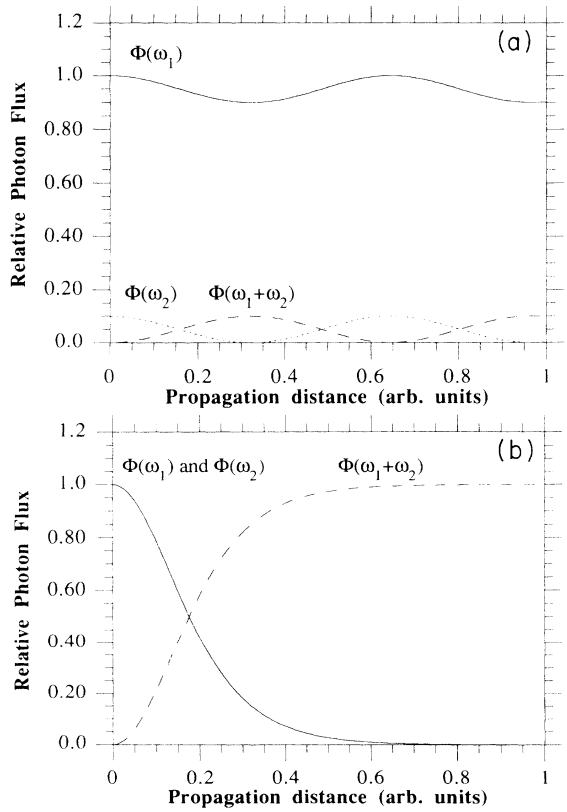

FIG. 1. Photon fluxes Φ_1, Φ_2, and Φ_3 at frequencies ω_1, ω_2, and $\omega_3=\omega_1+\omega_2$ vs propagation distance in the nonlinear crystal for SFG. The input fields taken to be real, $\Phi_3(z=0)=0$, and the effective nonlinear susceptibility is $\chi'=1.0$ (see text). (a) $\Phi_2(z=0)=\Phi_1(z=0)/10$. (b) $\Phi_2(z=0)=\Phi_1(z=0)$.

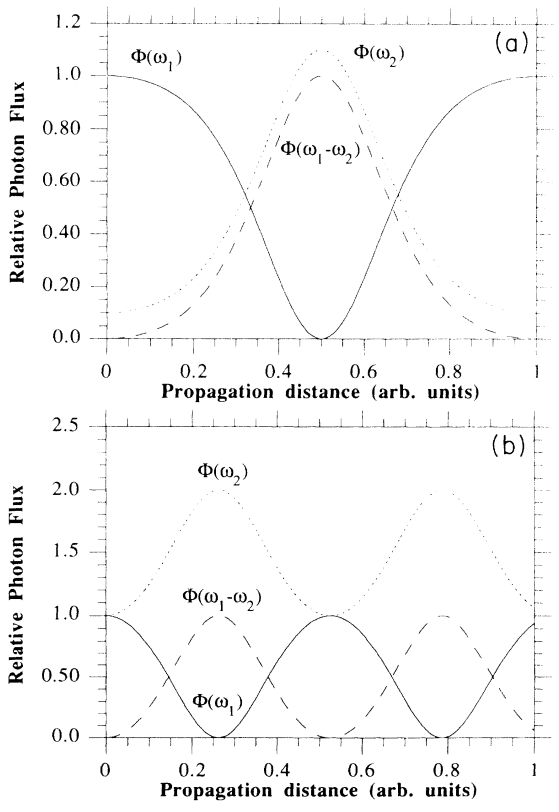

FIG. 2. Photon fluxes Φ_1, Φ_2, and Φ_3 at frequencies ω_1, ω_2, and $\omega_3=\omega_1-\omega_2$ vs propagation distance in the nonlinear crystal for DFG. The input fields taken to be real, $\Phi_3(z=0)=0$, and the effective nonlinear susceptibility is $\chi'=1.0$ (see text). (a) $\Phi_2(z=0)=\Phi_1(z=0)/10$. (b) $\Phi_2(z=0)=\Phi_1(z=0)$.

ith cavity), and $\theta_{i,j}$ are arbitrary phase shifts for the different modes. Hence the slowly varying envelope of the input field is given by

$$E_i(0,\tau)=\sum_{j=-n}^{n} E_{i,j}\exp[i(j\Delta_i\tau+\theta_{i,j})] \quad \text{for } i=1,2 .$$

As we shall see, the output spectrum can be much wider than the set of frequencies $\omega_{3,j,j'}=\omega_{1,j}\pm\omega_{2,j'}=\omega_1\pm\omega_2+\Delta_1 j\pm\Delta_2 j'$, where $j,j'=0,\ldots,n$. Moreover, the fundamental fields develop additional frequency components resulting from the depletion of photons when the photon flux of both input fundamental fields are simultaneously large, in a fashion similar to two-photon absorption [10]. This, of course, gives rise to additional frequency components of the output field. We take input fields each containing 11 equally spaced modes, with the slowly varying envelopes of the form

$$E_1(0,\tau)=\sum_{j=-5}^{5} E_{1,j}\exp[i(\Delta_1\tau+\theta_{1,j})] , \tag{12}$$

$$E_2(0,\tau)=\sum_{j=-5}^{5} E_{2,j}\exp[i(\Delta_2\tau+\theta_{2,j})] . \tag{13}$$

In our example, $\omega_1>\omega_2$ and the mode spacings of the two fields are taken to be 100 and 120 MHz, respectively ($\Delta_1=2\pi\times100\times10^6$ rad/s, $\Delta_1=2\pi\times120\times10^6$ rad/s). The amplitudes of the 11 modes $E_{1,j}$ are taken to be equal and the phases $\theta_{1,j}$ to be random in the interval $[0,2\pi]$ (generated by a random-number generator). The 11 modes $E_{2,j}$ are also taken to be equal and the phases $\theta_{2,j}$ to be random in the interval $[0,2\pi]$. Moreover, we take $\Phi_{1,j}=\Phi_{2,k}$ (i.e., $n_1E_{1,j}^2/\omega_1=n_2E_{2,k}^2/\omega_2$; the number of photons in each of the modes in both lasers are equal). Figure 3(a) shows the photon fluxes versus time for one particular realization of the phases $\theta_{1,j}$ and $\theta_{2,j}$. $\Phi_1(t)$ is cyclic with period 1×10^{-8} s, and $\Phi_2(t)$ is cyclic with period 1.2×10^{-8} s. Hence the dynamics is cyclic with period 6×10^{-8} s due to the commensurability of the mode spacing of the two fields. The time dependence of the flux is representative of mode-beating effects present in multimode lasers that are not mode locked. We calculate SFG and DFG using these input fields for low-, medium-, and high-frequency conversion, where low, medium, and high are defined by the effective parameters $\chi'L=0.001$, 0.1, and 1.0, respectively.

We first consider the temporal dependence of SFG. Figure 3 shows the output of the nonlinear crystal at frequencies ω_1, ω_2, and $\omega_3=\omega_1+\omega_2$ versus time for low conversion. The output at frequencies ω_1 and ω_2 are virtually indistinguishable from the input fields at these frequencies because the conversion is so low. The temporal profile of the output at the sum frequency is indistinguishable from the product of the photon fluxes at frequencies ω_1 and ω_2. When the intensity of one of the fields is low, the output at the sum frequency is also low, even if the intensity of the other input field is high, since significant intensity at both input fields is necessary for effective conversion. Hence the output $I(\omega_3)$ at $t=3.5\times10^{-9}$ s is small, despite the intensity at ω_1 being maximum, and output at ω_3 for $t=8.0\times10^{-9}$ s is large because the intensity at both ω_1 and ω_2 is high. The medium-conversion results are nearly identical to those in Fig. 3, except that the scale of the output at frequency ω_3 is about four orders of magnitude larger [$=100^2$, since the SFG flux is proportional to $(\Phi_1\Phi_2)^{1/2}\chi'L$ in the low conversion regime], because in the middle-conversion case, as in the low-conversion case, little depletion of the fundamental fields occurs. The high-conversion SFG presented in Fig. 4 is very different from the low- and

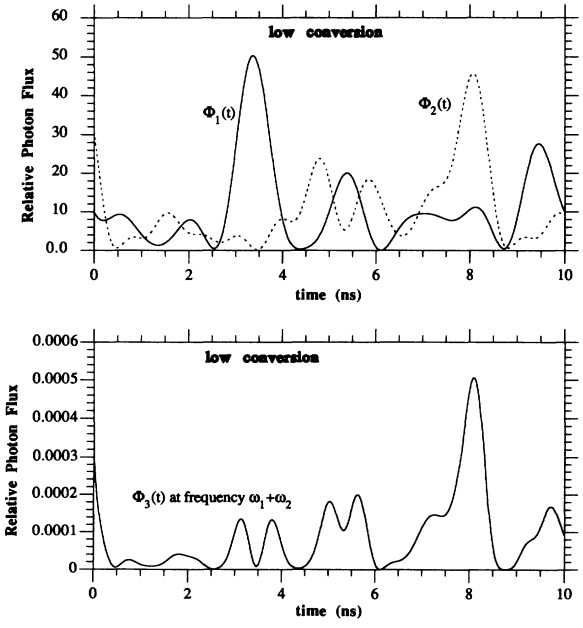

FIG. 3. Output of the nonlinear crystal at frequencies ω_1, ω_2, and $\omega_3=\omega_1+\omega_2$ vs time for low SFG conversion.

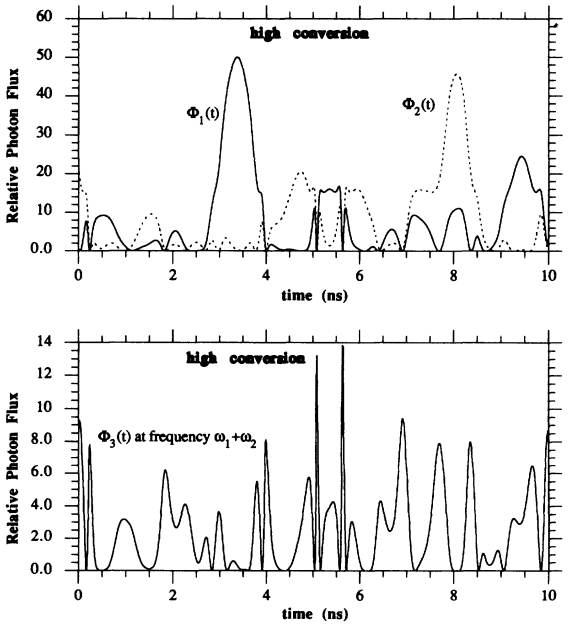

FIG. 4. Output of the nonlinear crystal at frequencies ω_1, ω_2, and $\omega_3=\omega_1+\omega_2$ vs time for high SFG conversion.

medium-conversion results. For example, at $t=8.0\times10^{-9}$ s the output at frequency $\omega_1+\omega_2$ nearly vanishes for high-frequency conversion, whereas for low and medium conversion, the output at frequency $\omega_1+\omega_2$ is maximum. The reason for the low output is the *reconversion* of $\omega_1+\omega_2$ photons to produce ω_1 and ω_2 photons. The temporal dependence of the high-conversion output at frequency $\omega_1+\omega_2$ clearly has more harmonic frequencies than the low or medium output at frequency $\omega_1+\omega_2$, i.e., the spectrum of the sum frequency is much richer. For low conversion there are $11\times11=121$ frequencies in the sum frequency. In the high-conversion output, additional frequencies result in the sum frequency because repeating depletion and reconversion of the input fields add additional frequency components to the fundamental fields, and these in turn add new frequencies to the sum frequency [1]. We conclude that in SFG, the input fluxes $\Phi_1(0,\tau)$ and $\Phi_2(0,\tau)$ and the output flux $\Phi_3(L,\tau)$ versus time are related in the following ways: (a) The output photon flux at τ is bounded by $\Phi_{\min}(0,\tau)$. (b) Only when both $\Phi_1(0,\tau)$ and $\Phi_2(0,\tau)$ are large can $\Phi_3(L,\tau)$ be large. (c) When both $\Phi_1(0,\tau)$ and $\Phi_2(0,\tau)$ are large, reconversion of ω_3 photons with the photons of the greater of the two input fields can occur, thereby reducing the output flux. (d) Some of the local maxima of the output flux occur when $\Phi_1(0,\tau)=\Phi_2(0,\tau)$, since at these points reconversion of ω_3 photons with the photons of the greater of the two input fields cannot occur. These points are clearly illustrated in Fig. 5, which plots the photon input fluxes and output flux $\Phi_3(L,\tau)$ on the same figure for the high conversion case.

We now consider DFG. The output of the nonlinear crystal at frequencies ω_1, ω_2, and $\omega_3=\omega_1-\omega_2$ versus time for low conversion are almost indistinguishable from the low-conversion results for SFG shown in Fig. 3; this despite the different nature of the processes [for SFG, ω_1 photons$+\omega_2$ photons$\rightarrow\omega_3$ photons, whereas for DFG, ω_1 photons$\rightarrow\omega_2$ photons$+\omega_3$ $(=\omega_1-\omega_2)$ photons]. Hence we do not plot these results. Figure 6 shows the results for medium conversion. Here, some differences

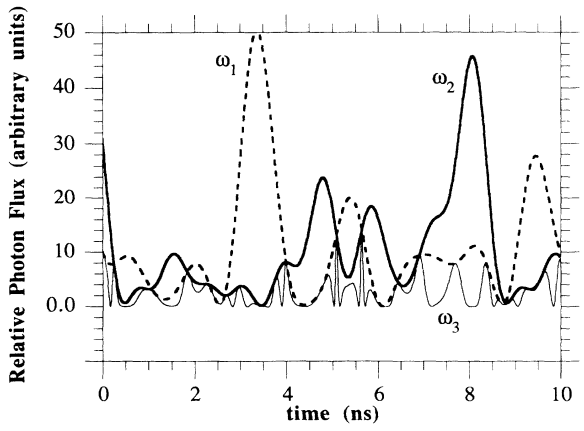

FIG. 5. Output of the nonlinear crystal at frequencies ω_1, ω_2, and $\omega_3=\omega_1+\omega_2$ vs time for high SFG conversion plotted on the same graph.

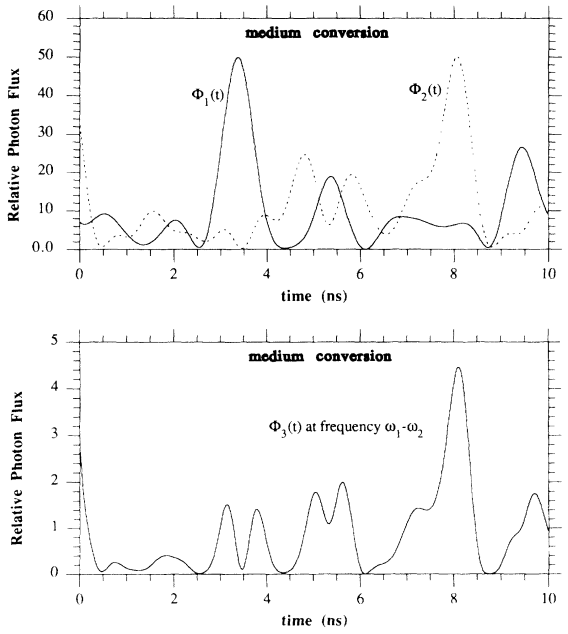

FIG. 6. Output of the nonlinear crystal at frequencies ω_1, ω_2, and $\omega_3=\omega_1-\omega_2$ vs time for medium DFG conversion.

(in addition to the change of scale for the sum frequency) can be seen from the low-conversion DFG case. The peak of the ω_2 photon flux at $t=8.0\times10^{-9}$ s is clearly larger than in the weak-conversion regime due to effective DFG, which produces both ω_2 and $\omega_1-\omega_2$ photons. Hence the medium-conversion results for DFG are in the regime where pump depletion is beginning to affect the dynamics. Figure 7 shows the photon fluxes after passing through the nonlinear crystal versus time for

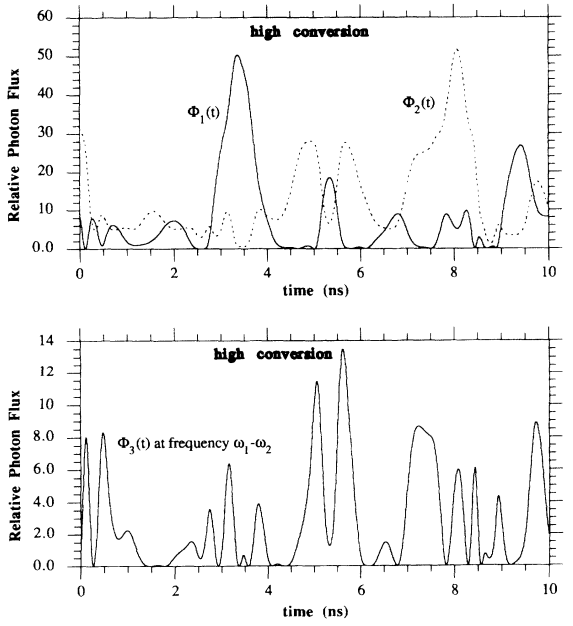

FIG. 7. Output of the nonlinear crystal at frequencies ω_1, ω_2, and $\omega_3=\omega_1-\omega_2$ vs time for high DFG conversion.

high conversion. This result is dramatically different from the low- and medium-conversion regimes, and is also radically different from the high-conversion SFG result. The different nature of the dynamics of SFG and DFG is thereby underscored. We conclude that in DFG, the input flux $\Phi_1(0,\tau)$ and the output fluxes $\Phi_1(L,\tau)$, $\Phi_2(L,\tau)$, and $\Phi_3(L,\tau)$ are related in the following ways: (a) The output photon flux at τ is bounded by the smaller of $\Phi_1(0,\tau)$ and $\Phi_2(L,\tau)$. (b) Only when both $\Phi_1(0,\tau)$ and $\Phi_2(L,\tau)$ (the flux of photons at frequency ω_2 at the *end* of the nonlinear medium) are large can $\Phi_3(L,\tau)$ be large (this is a necessary but not a sufficient condition). (d) The maxima of the output flux $\Phi_3(L,\tau)$ occur when $\Phi_1(0,\tau)-\Phi_1(L,\tau)$ is maximum [but this is obvious since this difference equals $\Phi_3(L,\tau)$].

The quantum efficiencies for SFG and DFG, defined as $\eta_{\text{quant}}=\{N(\omega_3)_{\text{output}}/[N(\omega_1)+N(\omega_2)]_{\text{input}}\}$, where $N(\omega_i)$ indicates the number of photons at frequencies ω_i, calculated using the input fields used to obtain Figs. 1–6, are presented in Table I. At low conversion, the quantum efficiencies of SFG and DFG are nearly equal (provided the nonlinear susceptibilities for SFG and DFG are equal). However, the DFG quantum efficiency is higher than that of SFG for significant conversion. When a small number of photons at frequency ω_2 is initially presented and a significant number of ω_1 photons is present, DFG generates additional ω_2 photons (at the same rate as production of photons of frequency ω_3) necessary to further catalyze the DFG process. However, for SFG, ω_2 photons are removed. Hence the increase in the number of ω_2 photons for DFG increase the quantum efficiency whereas the decrease of the number of ω_2 photons decreases the quantum efficiency.

The energy efficiency for the three-wave-mixing process, defined as $\eta_{\text{energy}}=\{W(\omega_3)_{\text{output}}/[W(\omega_1)+W(\omega_2)]_{\text{input}}\}$, where $W(\omega_i)=\hbar\omega_i N(\omega_i)$ indicates the energy of the photon field at the central frequency ω_i, is related to the $N(\omega_i)$ through the equation

$$\eta_{\text{energy}}=\frac{W(\omega_3)_{\text{output}}}{[W(\omega_1)+W(\omega_2)]_{\text{input}}}=\frac{\omega_3 N(\omega_3)_{\text{output}}}{[\omega_3 N(\omega_1)+\omega_2 N(\omega_2)]_{\text{input}}}\ . \tag{14}$$

DFG energy efficiencies are adversely affected when the difference frequency $\omega_3=\omega_1-\omega_2$ is small. Hence, even if the quantum efficiency of DFG is high, the energy efficiency is very low if the input frequencies are in the visible and the difference frequency is in the infrared.

TABLE I. Quantum efficiency for SFG and DFG. Equal numbers of photons in both input fields, and random phases for the 11 modes in each input beam, are selected.

Relative intensity	SFG	DFG
Low	4.0×10^{-6}	4.0×10^{-6}
Medium	0.037	0.041
High	0.117	0.134

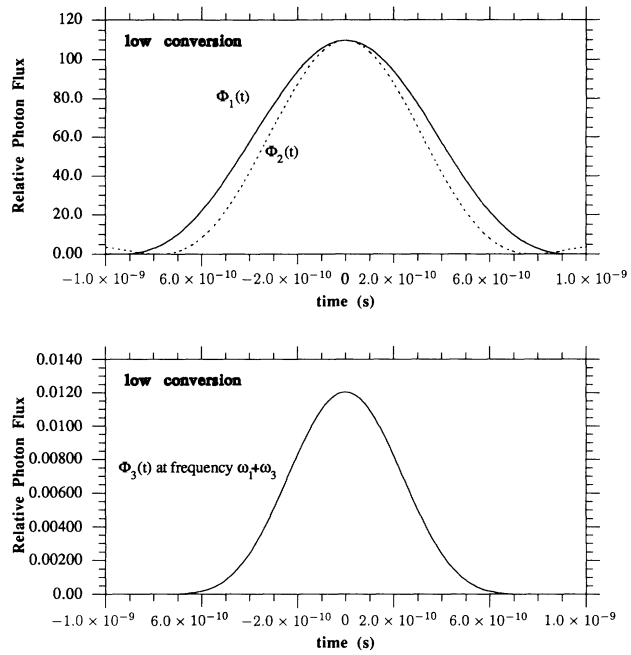

FIG. 8. Output of the nonlinear crystal at frequencies ω_1, ω_2, and $\omega_3=\omega_1+\omega_2$ vs time for low SFG conversion for mode-locked input pulses.

We now present SFG and DFG results for mode-locked pulses. Figure 8 shows the input pulses at ω_1 and ω_2 for and the sum-frequency output at $\omega_1+\omega_2$ for low conversion. Again, the DFG at low conversion is almost identical to the SFG results. Figures 9 and 10 show output pulses at ω_1, ω_2, and $\omega_1+\omega_2$ at medium and high con-

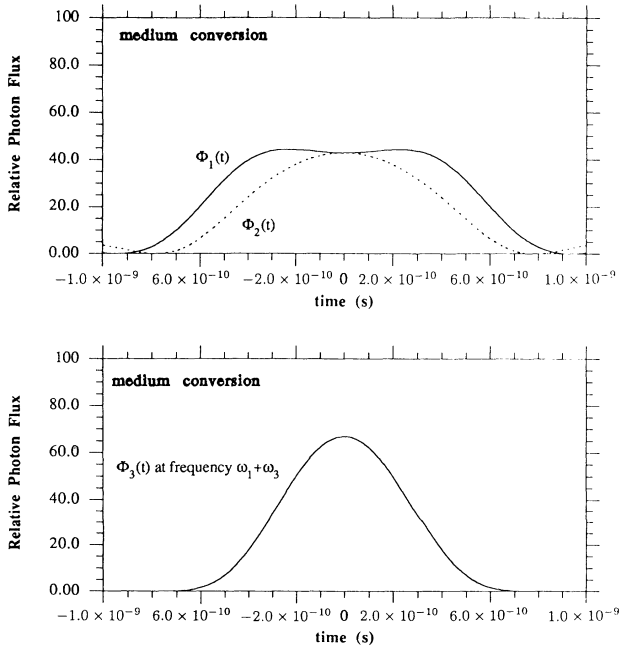

FIG. 9. Output of the nonlinear crystal at frequencies ω_1, ω_2, and $\omega_3=\omega_1+\omega_2$ vs time for medium SFG conversion for mode-locked input pulses.

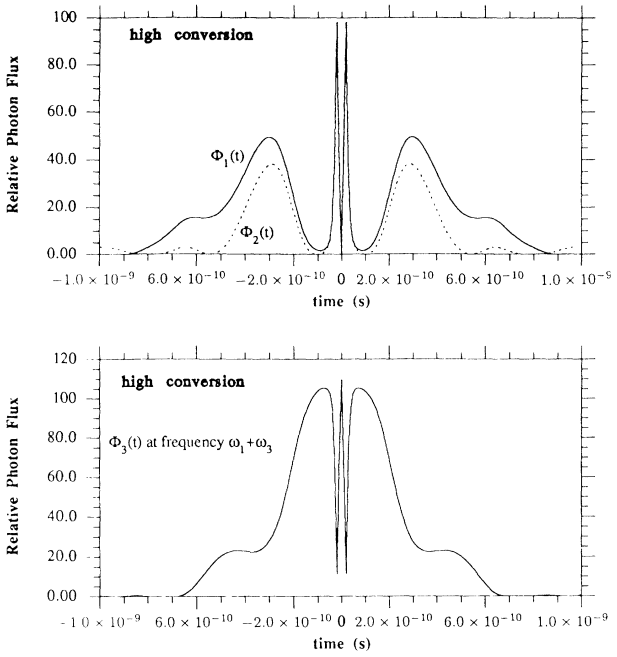

FIG. 10. Output of the nonlinear crystal at frequencies ω_1, ω_2, and $\omega_3=\omega_1+\omega_2$ vs time for high SFG conversion for mode-locked input pulses.

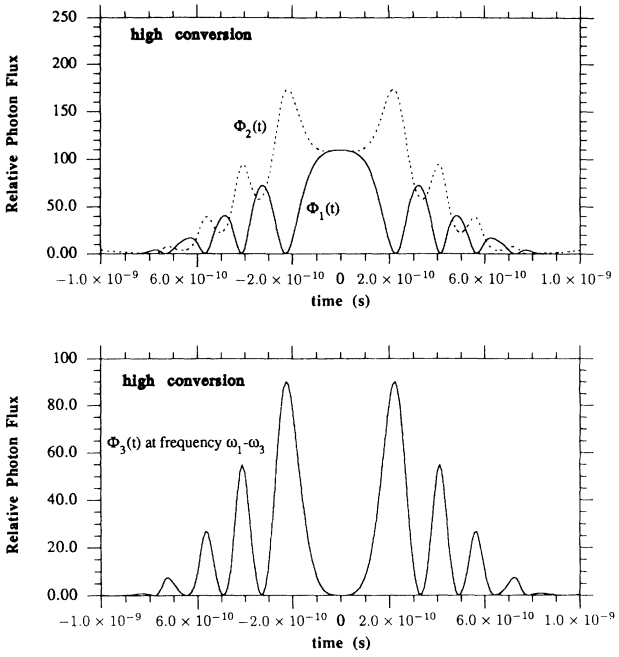

FIG. 12. Output of the nonlinear crystal at frequencies ω_1, ω_2, and $\omega_3=\omega_1+\omega_2$ vs time for high DFG conversion for mode-locked input pulses.

version, respectively. At medium conversion, the depletion of the peaks of the input pulses is apparent. At high conversion, the pulse depletion and the reconversion process are dramatic. Figures 11 and 12 show output pulses at ω_1, ω_2, and $\omega_1-\omega_2$ at medium and high conversion, respectively, for DFG. At medium conversion, the depletion of the peak of the ω_1 pulse and the corresponding buildup of the ω_2 and ω_3 pulses is evident. At high conversion, the pulse depletion of the ω_1 pulse, buildup of the ω_1 and ω_2 pulses, and the reconversion processes are significantly different in character than for SFG.

It is interesting to compare the results of SFG and DFG for input fields that are amplitude and phase modu-

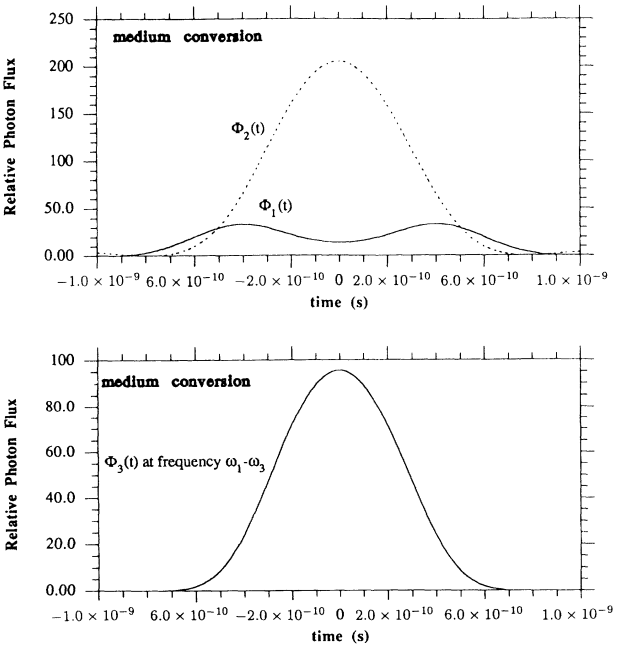

FIG. 11. Output of the nonlinear crystal at frequencies ω_1, ω_2, and $\omega_3=\omega_1-\omega_2$ vs time for medium DFG conversion for mode-locked input pulses.

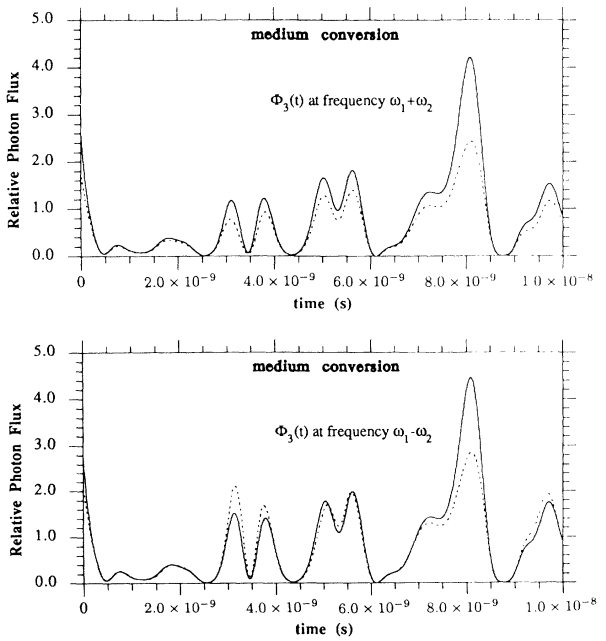

FIG. 13. Output of the nonlinear crystal at frequency $\omega_3=\omega_1+\omega_2$ for SFG and $\omega_3=\omega_1-\omega_2$ for DFG for the medium-conversion case. For the dashed curves, the self-phase modulation susceptibility for the field at frequency ω_1 is taken to be nonzero and arbitrarily set equal to the SFG susceptibility, $\chi_{\rm pm}(-\omega_1;\omega_1,-\omega_1,\omega_1)=\chi'$.

lated with those for input fields with the same amplitude modulation but incorporate no phase modulation. To second order in the nonlinear interaction, phase modulation does not affect the SFG and DFG dynamics. To prove this, we develop the perturbation theory for SFG and DFG. We write the incident fields [see Eq. (4)] as

$$\begin{aligned}\phi_1(0,\tau)&=|\phi_1(0,\tau)|\exp[i\theta_1(0,\tau)]\ ,\\ \phi_2(0,\tau)&=|\phi_2(0,\tau)|\exp[i\theta_2(0,\tau)]\ .\end{aligned}\tag{15}$$

Using Eq. (4) for SFG [Eq. (11) for DFG], we find the first-order perturbation theory result,

$$\begin{aligned}\phi_3(z,\tau)=&-i\chi'|\phi_1(0,\tau)||\phi_2(0,\tau)|\\ &\times\exp\{i[\theta_1(0,\tau)+\theta_2(0,\tau)]\}z \quad \text{for SFG}\ ,\\ \phi_3(z,\tau)=&-i\chi'|\phi_1(0,\tau)||\phi_2(0,\tau)|\\ &\times\exp\{i[\theta_1(0,\tau)-\theta_2(0,\tau)]\}-z \quad \text{for DFG}\ .\end{aligned}\tag{16}$$

Upon substituting these expressions back into Eq. (4) [(11)], we obtain the second-order interaction expressions for the fundamental fields for SFG (DFG),

$$\begin{aligned}\phi_1(z,\tau)=&\exp[i\theta_1(0,\tau)]|\phi_1(0,\tau)|\\ &\times[1-\chi'^2|\phi_1(0,\tau)||\phi_2(0,\tau)|z^2/2]\ ,\\ \phi_2(z,\tau)=&\exp[i\theta_2(0,\tau)]|\phi_2(0,\tau)|\\ &\times[1-\chi'^2|\phi_1(0,\tau)||\phi_2(0,\tau)|z^2/2]\ .\end{aligned}\tag{17}$$

Hence, to first order, the magnitude of the field and frequency ω_3 does not depend upon the phases of the input fields [as is clear from Eq. (16)] and, to second order, the phases of the input fields remain unchanged upon propagation through the crystal [Eq. (17)]. This result holds to arbitrary order. To demonstrate that the amplitude of the field and frequency ω_3 does not depend upon the phases of the input fields to higher order, we calculate SFG and DFG for (a) input fields that are amplitude and phase modulated and (b) input fields with the same amplitude modulation but incorporate no phase modulation. We use the slowly varying envelopes of the input fields of Eqs. (12) and (13) and compare the results with those obtained using the absolute values of the input fields in Eqs. (12) and (13). The latter input fields are only amplitude modulated, yet have an identical intensity to previous input fields. For low, medium, and high conversion, the results for both SFG and DFG intensities were indistinguishable from each other. The practical application of this is that, for arbitrary input field modulation, one can remove the phase modulation of the fields, compute the output intensities of the purely amplitude-modulated fields using the analytic formulas presented in Sec. II, and thereby obtain correct output-field intensities for the original input fields with arbitrary modulation.

Given that phase modulation of the input fields has no effect on the output intensities for the SFG and DFG conversion processes, it is of interest to determine the effect of self- and cross-phase modulation upon these processes. The set of dynamical equations governing SFG including self- and cross-phase-modulation terms are as follows:

$$\begin{aligned}\frac{\partial\phi_1(z,\tau)}{\partial z}&=-i\chi'\phi_3\phi_2^*-i[\chi_{\rm pm}(-\omega_1;\omega_1,-\omega_1,\omega_1)|\phi_1|^2+2\chi_{\rm pm}(-\omega_1;\omega_2,-\omega_2,\omega_1)|\phi_2|^2+2\chi_{\rm pm}(-\omega_1;\omega_3,-\omega_3,\omega_1)|\phi_3|^2]\phi_1\ ,\\ \frac{\partial\phi_2(z,\tau)}{\partial z}&=-i\chi'\phi_3\phi_1^*-i[\chi_{\rm pm}(-\omega_2;\omega_2,-\omega_2,\omega_2)|\phi_2|^2+2\chi_{\rm pm}(-\omega_2;\omega_1,-\omega_1,\omega_2)|\phi_1|^2+2\chi_{\rm pm}(-\omega_2;\omega_3,-\omega_3,\omega_2)|\phi_3|^2]\phi_2\ ,\\ \frac{\partial\phi_3(z,\tau)}{\partial z}&=-i\chi'\phi_1\phi_2-i[\chi_{\rm pm}(-\omega_3;\omega_3,-\omega_3,\omega_3)|\phi_3|^2+2\chi_{\rm pm}(-\omega_3;\omega_1,-\omega_1,\omega_3)|\phi_1|^2+2\chi_{\rm pm}(-\omega_3;\omega_2,-\omega_2,\omega_3)|\phi_3|^2]\phi_3\ .\end{aligned}\tag{18}$$

Self-phase modulation is a higher-order process than SFG or DFG. Only when the electric fields are large and the phase modulation susceptibilities $\chi_{\rm pm}$ are sufficiently large does phase modulation play a significant role. Figure 13 shows the output of the nonlinear crystal at frequency $\omega_3=\omega_1+\omega_2$ for the medium-conversion SFG case and at frequency $\omega_3=\omega_1-\omega_2$ for medium-conversion DFG, where the self-phase modulation susceptibility for the field at frequency ω_1 is taken to be nonzero and arbitrarily set equal to the SFG susceptibility, $\chi_{\rm pm}(-\omega_1;\omega_1,-\omega_1,\omega_1)=\chi'$, and all the remaining third-order nonlinear susceptibilities are made to vanish. Figure 14 shows the output of the nonlinear crystal at frequency $\omega_3=\omega_1+\omega_2$ for SFG and the nonlinear crystal at frequency $\omega_3=\omega_1-\omega_2$ for DFG for the high-conversion case. The results including self-phase modulation are indicated by dashed curves, and the solid curves are the results without phase modulation. There is clearly an effect due to the self-phase modulation. In SFG, the self-phase modulation reduces the output at the sum-frequency intensity because the phase modulation serves to ruin the phase matching of the fundamental fields in the crystal. Inclusion of additional nonvanishing self- and cross-phase modulation susceptibilities further reduces the SFG. In DFG, the self-phase modulation can increase or decrease the difference-frequency intensity. Details of

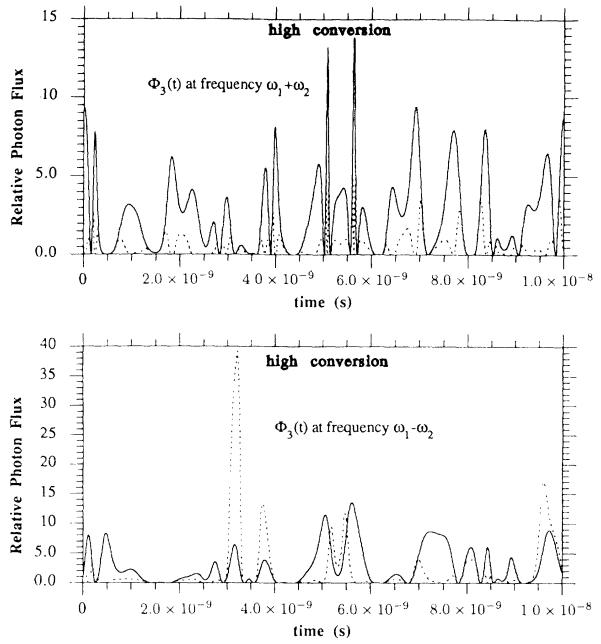

FIG. 14. Same as Fig. 13, except for the high-conversion case.

when there is an increase and when there is a decrease remain to be studied.

IV. IMPROVED SFG USING DELAY LINES

In Ref. [8] we described the experimental demonstration of a scheme for improving the efficiency of SFG for broadband input fields based on an idea originally presented in Ref. [1]. The method involves using an arrangement with two or more nonlinear mixing crystals and a time-delay line for one of the fundamental fields situated between the crystals, which temporally shifts the fundamental fields one relative to another before they enter the next nonlinear crystal. The improvement in efficiency for SFG using the method is substantial, particularly when the efficiency of SFG in the first crystal was significant. However, the improvement of DFG efficiency is minimal. In the experiment, the two SFG input beams were generated by excimer laser pumped dye lasers, each consisting of an oscillator and amplifier. Molectron DL 200 dye lasers were used as oscillators with Coumarin 480 and Rhodamine 6G dyes generating light at 480 and 575 nm, respectively. The output beams from the oscillators were spatially filtered and amplified using prism dye cells of Bethune design [11] to achieve high-quality optical beams. The maximum output energy from the amplifiers was close to 2 mJ, with pulse duration of 10 ns. The bandwidths of the lasers were approximately 7 GHz and the mode spacing was 375 MHz. Care was taken to avoid saturation in the oscillators and amplifiers leading to mode coupling and non-Gaussian statistics. The lack of significant mode coupling was verified experimentally by measuring the second-order autocorrelation function of the laser light [12]. Figure 15 shows the autocorrelation function for the 575-nm laser. Peak values of

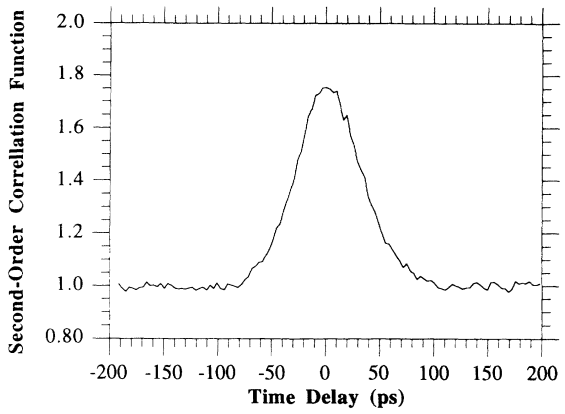

FIG. 15. Autocorrelation function for the 575-nm laser.

the autocorrelation functions for the output of the oscillator and amplifier of 575- and 480-nm lasers are equal to 1.75 while the theoretical value for our lasers is close to 1.9, assuming a Gaussian line shape [13]. This indicates the presence of rather weak residual mode coupling in the oscillators. However, such a laser tends to operate with a smaller number of modes on each particular pulse than indicated by the average linewidth [14]. The peak value of the autocorrelation function is thereby lowered. The data also show that the intensity fluctuations are not significantly changed in the amplifiers. Hence the lasers were almost free of nonlinear mode coupling and, to a good approximation, can be modeled as operating with several independent modes with random phases as in our theoretical model. The width of the autocorrelation function, corresponding to the coherence time of the laser, is about 60 ps. The two input beams for DFG were at 364 and 575 nm, respectively, yielding a difference frequency of 980 nm.

Figure 16 shows the SFG efficiency of the second nonlinear crystal, η_2, versus time delay τ between the ω_1 and ω_2 beams. The data are normalized to unity for time delay $\tau=0$. The four curves correspond to different conversion efficiencies in the first nonlinear crystal, η_1, ranging

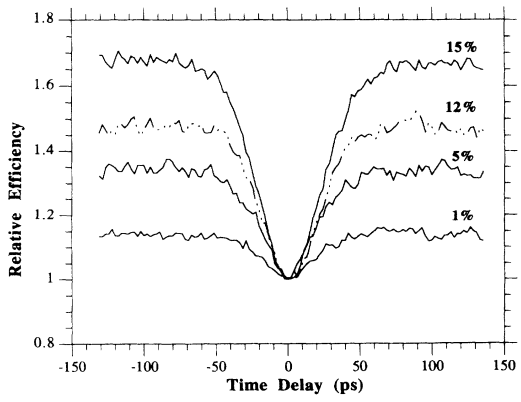

FIG. 16. SFG efficiency of the second nonlinear crystal, η_2, vs time delay τ between the ω_1 and ω_2 beams.

from 15% to 1%, obtained by decreasing the input intensity of the ω_1 beam with neutral density filters. Clearly, η_2 increases with $|\tau|$ for all curves. The width of the region of increase of the curves is comparable to the coherence time of the laser beams. The efficiency η_2 approaches a constant value independent of $|\tau|$ for time delay much longer than the coherence time, and the constant value depends on the conversion efficiency η_1 of the fist crystal, with larger η_1 yielding larger increase of η_2. In the experiment, at $\eta_1=15\%$, sufficiently large time delay increased conversion efficiency of the second crystal by 70% over the result with $\tau=0$, and η_2 approaches the conversion efficiency of the first crystal, η_1, if τ is large. The DFG efficiency of the second nonlinear crystal, η_2, versus time delay τ is flat within experimental error. Hence no improvement of efficiency is obtained for the DFG case.

These results can be understood in terms of the theory of SFG and DFG presented in Secs. II and III. Since both input laser beams have intensities fluctuating randomly and independently, the temporal regions of overlapping high intensities in both beams are stochastic. The first nonlinear crystal eliminates these mutually correlated intensity fluctuations by converting them into intensity at the sum frequency. As a result, the fundamental laser beams after the first crystal are temporally anticorrelated. The anticorrelation of the laser beams reduces conversion efficiency in the second crystal if no time delay is between the fundamental beams is allowed for, despite the fact that the average intensities are still high. By introducing a time delay τ longer than the coherence time, the anticorrelation is destroyed and conversion efficiency in the second crystal is restored. The η_2 vs τ dependence is a measure of the intensity cross-correlation between the two laser beams. The experimental results presented in Fig. 16 indicate that, upon leaving the first crystal, the laser beams are anticorrelated due to the nonlinear wave mixing with anticorrelation more pronounced for higher conversion efficiency. The lack of improvement of efficiency for DFG in our experiment is due to two reasons. First, the calculated improvement of efficiency for DFG is much smaller than for SFG because the DFG process destroys ω_1 photons but generates ω_2 photons so the product of ω_1 and ω_2 photons is not as dramatically affected (in the low-conversion efficiency regime, DFG is proportional to the product). Second, the DFG process does not require that the intensity of the ω_1 and ω_2 beams both be high for efficient conversion, and the time-delay process is designed to increase the chance that both beams simultaneously have high intensity.

Figure 17 shows the results of modeling the experiment by passing the pulses used in Fig. 7 through two crystals. We use the high-conversion efficiency parameters to accentuate the differences with and without decay. The figure shows the relative photon flux at various stages of traversing a system containing two nonlinear crystals separated by a delay line for one of the crystals. The first two frames in the figure are identical to those of Fig. 7 and show the input at frequencies ω_1 and ω_2 and the output of the first crystal at frequency ω_3, respectively. The third frame shows the output at the fundamental frequencies ω_1 and ω_2 upon emerging from the first crystal. The fourth frame shows the resulting output at the sum frequency ω_3 upon emerging from the second crystal. In temporal regions where the fundamental fields are significantly depleted, the sum-frequency output intensity of the second is not large. The fifth frame shows the output at ω_3 upon emerging from the second crystal if a time delay of 1 ns of the beam at frequency is applied to the ω_2 beam. Clearly, the output intensity obtained upon temporally delaying the ω_2 beam as shown in the fifth frame

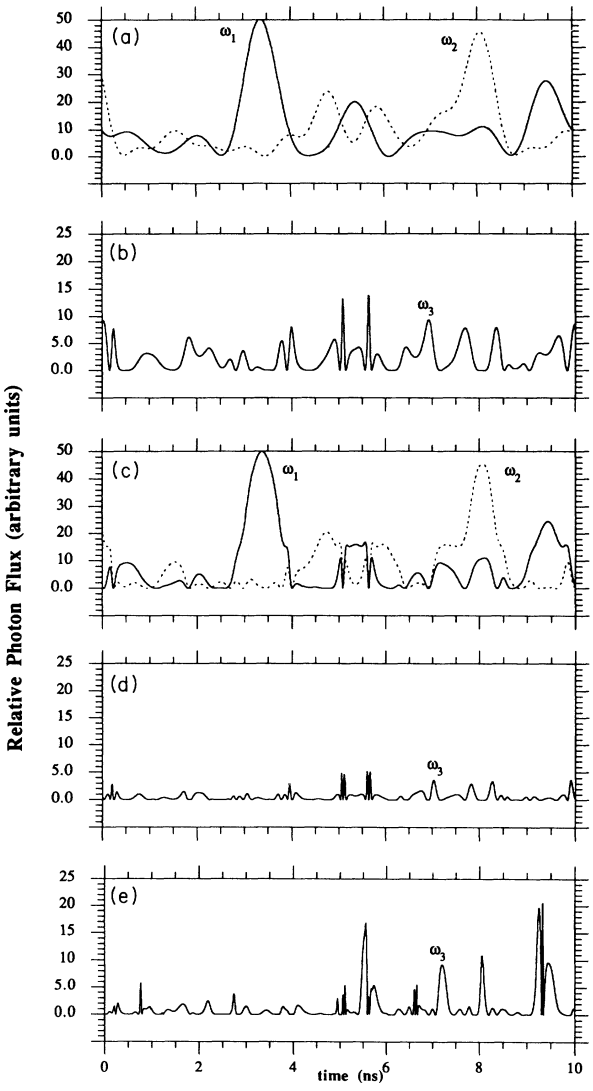

FIG. 17. Relative photon flux at various stages of traversing a system containing two nonlinear crystals separated by a delay line for one of the crystals. (a) Input at frequencies ω_1 and ω_2; (b) output of the first crystal at frequency ω_3, respectively; (c) output at the fundamental frequencies ω_1 and ω_2 upon emerging from the first crystal; (d) output at the sum frequency ω_3, upon emerging from the second crystal; (e) output at ω_3 upon emerging from the second crystal when the time delay of 1 ns of the beam at frequency is applied to the ω_2 beam.

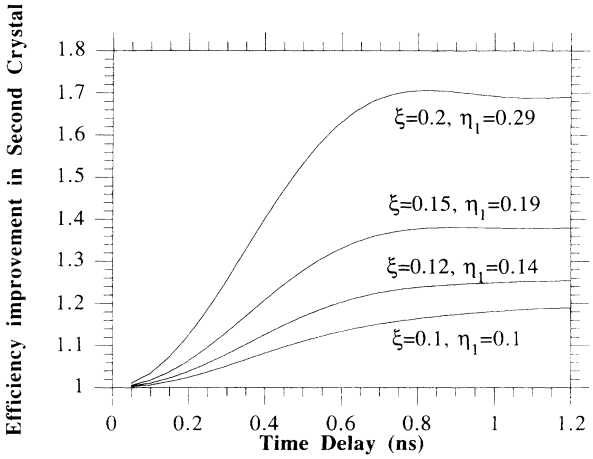

FIG. 18. Improvement of efficiency η_2 vs time delay τ for four different values of η_1.

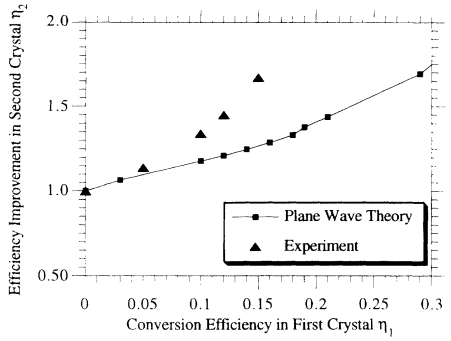

FIG. 20. η_2 vs η_1 (for sufficiently large time delay) obtained experimentally and theoretically.

is larger than without delay in the fourth frame. The peaks of the input pulses impinging on the second crystal now have a chance of overlapping well, and greater conversion is obtainable from the second crystal than in the case without time delay.

Figure 18 shows the improvement of efficiency versus time delay for four different values of $\xi \equiv \Phi^{1/2}\chi' L$, i.e., $\xi = 0.1$, 0.12, 0.15, and 0.2, corresponding to efficiencies of conversion in the first crystal of $\eta_1 = 0.1$, 0.14, 0.19, and 0.29, respectively. In these calculations we took $\Phi = \Phi_1 = \Phi_2$, i.e., equal average photon flux in both input beams [$\Phi_i = cn_i|E_i|^2/\hbar\omega_i$, $\chi' = (\hbar^3\omega_1\omega_2\omega_3/c^3 n_1 n_2 n_3)^{1/2}\chi$ is the modified nonlinear susceptibility, and L is the nonlinear crystal length]. We averaged over many random choices of the phases $\theta_{1,j}$ and $\theta_{2,j}$ of the field modes to collect the statistics shown in the numerical calculations. The results in Fig. 18 are similar to those obtained experimentally in that the efficiency increases with increasing efficiency in the first crystal and increasing time delay up to the coherence time of the laser field. However, here the mode spacing in the numerical calculations is smaller than for the experimental beams, hence the coherence time is longer. Also, in these calculations, the average flux in both input beams was taken to be equal, whereas in the experiments, the average flux in one of the laser beams was decreased. Hence we expect higher efficiency in the theoretical calculations because the highest conversion efficiency occurs when there are equal numbers of photons of frequency ω_1 and ω_2. Figure 19 shows the improvement of efficiency in the second crystal versus $\Phi^{1/2}\chi' L$ for SFG and DFG. Clearly, there is substantial improvement of the efficiency for SFG for sufficiently large nonlinearity, however the DFG efficiency improvement for realistic intensities is modest at best, as confirmed by our experiment. For $\Phi^{1/2}\chi' L > 0.3$, significant reconversion occurs in both crystals; hence the dropoff of η_2 with increasing $\Phi^{1/2}\chi' L$. Figure 20 plots η_2 vs η_1 (for sufficiently large time delay) obtained experimentally and theoretically. The same general trend is obtained in both the experiment and the numerical results. It is somewhat surprising that the experimental results have greater efficiency improvement than the theoretical results, but one must keep in mind that the theoretical results are not an exact simulation of the experiment. De-

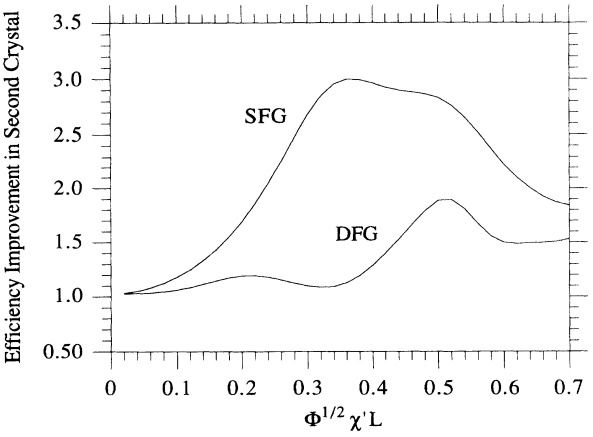

FIG. 19. Improvement of efficiency in the second crystal vs $\Phi^{1/2}\chi' L$ for SFG and DFG.

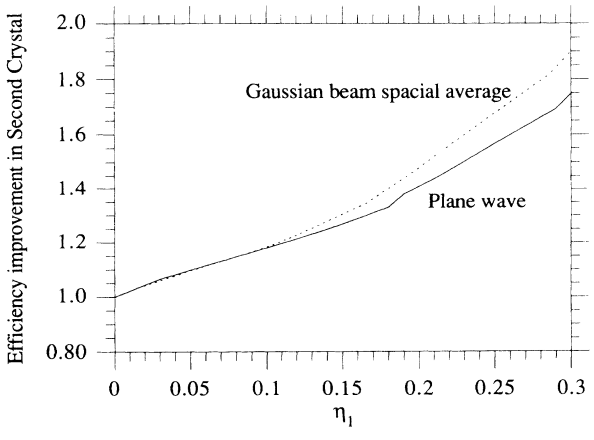

FIG. 21. Simulation of η_2 vs η_1 (for sufficiently large time delay) obtained upon simulating a spatial Gaussian beam profile.

tailed comparison with experiment would require inclusion of spatial mode profiles of the beams and the effects of beam walkoff. To simulate the effects of a spatial Gaussian beam profile, we appropriately averaged over intensity of the incident beam with Gaussian weights to obtain the results shown in Fig. 21. This figure demonstrates that the results for η_2 vs η_1 is not very sensitive to the Gaussian spatial average of the beams until η_1 exceeds about 0.2. We have not tried to simulate the effects of beam walkoff.

V. SUMMARY AND CONCLUSION

We presented the theoretical framework for the analysis of sum- and difference-frequency generation of broadband input fields. For SFG, the input fluxes $\Phi_1(0,\tau)$ and $\Phi_2(0,\tau)$ and the output flux $\Phi_3(L,\tau)$ versus time are related as follows: (a) The output photon flux at τ is bounded by $\Phi_{\min}(0,\tau)$. (b) Only when both $\Phi_1(0,\tau)$ and $\Phi_2(0,\tau)$ are large can $\Phi_3(L,\tau)$ be large. (c) When both $\Phi_1(0,\tau)$ and $\Phi_2(0,\tau)$ are large, reconversion of ω_3 photons with the photons of the greater of the two input fields can occur, thereby reducing the output flux. (d) Some of the local maxima of the output flux occur when $\Phi_1(0,\tau)=\Phi_2(0,\tau)$, since at these points reconversion of ω_3 photons with the photons of the greater of the two input fields cannot occur. For DFG, the input flux $\Phi_1(0,\tau)$ and the output fluxes $\Phi_1(L,\tau)$, $\Phi_2(L,\tau)$, and the $\Phi_3(L,\tau)$ are related in the following ways: (a) The output photon flux at τ is bounded by the smaller of $\Phi_1(0,\tau)$ and $\Phi_2(L,\tau)$. (b) Only when both $\Phi_1(0,\tau)$ and $\Phi_2(L,\tau)$ (the flux of photons at frequency ω_2 at the *end* of the nonlinear medium) are large can $\Phi_3(L,\tau)$ be large (this is a necessary but not a sufficient condition). (c) The maxima of the output flux $\Phi_3(L,\tau)$ occur when $\Phi_1(0,\tau)-\Phi_1(L,\tau)$ is maximum.

The efficient sum-frequency generation for broadband input fields that was experimentally demonstrated [8] is theoretically analyzed. The method involves using an arrangement with two or more nonlinear mixing crystals with a time-delay line, situated between the crystals, for one of the fundamental fields relative to the other. The delay line temporally shifts the fundamental fields one relative to another by a time longer than their coherence time. The improvement in efficiency for SFG using the method is much higher than for difference-frequency generation. Experimentally, the conversion efficiency of the second crystal is increased almost to that of the first crystal by time-delaying one of the input fields, thereby eliminating the anticorrelation caused by the SFG in the first crystal. Additional stages can be cascaded using this approach. The time-delay method is not effective for mutlimode DFG.

[1] Y. B. Band, D. F. Heller, and J. S. Krasinski, Phys. Rev. A **40**, 4400 (1989); in *Coherence and Quantum Optics VI,* edited by J. H. Eberly, L. Mandel, and E. Wolf (Plenum, New York, 1990), pp. 77–82.

[2] Y. B. Band, D. F. Heller, J. R. Ackerhalt, and J. Krasinski, Phys. Rev. A **42**, 1515 (1990).

[3] J. A. Armstrong, N. Bloembergen, J. Ducuing, and P. S. Pershan, Phys. Rev. **127**, 1918 (1962).

[4] N. Bloembergen, *Nonlinear Optics* (Benjamin, New York, 1965).

[5] Y. R. Shen, *The Principles of Nonlinear Optics* (Wiley, New York, 1984), pp. 67–140.

[6] A. Yariv, *Quantum Electronics,* 3rd ed. (Wiley, New York, 1975).

[7] Y. B. Band, J. Ackerhalt, and J. Krasinski, Phys. Rev. A **43**, 1528 (1990); Y. B. Band, D. E. Grosjean, and J. S. Krasinski, IEEE J. Quantum Electron. **QE-28**, 1400 (1992); Opt. Lett. **16**, 726 (1991).

[8] C. Radzewicz, J. S. Krasinski, and Y. B. Band, Opt. Lett. **18**, 331 (1993).

[9] *Handbook of Mathematical Functions,* Natl. Bur. Stand. Appl. Math. Ser. No. 55, edited by M. Abramowitz and I. A. Stegun (U.S. GPO, Washington, D.C., 1964), pp. 569–581.

[10] H. P. Weber, IEEE J. Quantum Electron. **QE-7**, 189 (1971).

[11] D. S. Bethune, Appl. Opt. **20**, 1897 (1981).

[12] R. J. Glauber, Phys. Rev. **130**, 2529 (1963).

[13] A. V. Masalow and S. S. Todirashku, Opt. Commun. **32**, 497 (1980).

[14] L. A. Westling and M. G. Raymer, J. Opt. Soc. Am. **3**, 911 (1986).